One-Dimensional Hubbard Model in High Temperatures Through Many-Body Perturbation Theory

M.A. Tag[a,*] and A. Hafdallah[b]

[a] *Computational Physics and Quantum Phenomena Laboratory (CPQPL), Echahid Cheikh Larbi Tebessi University, Tebessa, Algeria*
[b] *LPAT Laboratory, Echahid Cheikh Larbi Tebessi University, Tebessa, Algeria*

Received: 07.10.2024 & Accepted: 11.12.2024

Doi: 10.12693/APhysPolA.147.79 *e-mail: mohamed.tag@univ-tebessa.dz

We present symbolic algorithms designed to investigate the perturbative expansions of the d-Hubbard model. These methods are part of recent developments in many-body perturbation theory that aim to reformulate Feynman diagrams in terms of divided differences. The direct application of this technique to the one-dimensional Hubbard model yields the coefficients of the grand potential up to the sixth order, expressed in terms of both the interacting potential (U expansions) and high-temperature expansions (β expansions). A key feature of this approach is the ability to merge the β expansions to any desired order. To verify our analytical results, we compare the derived magnetic susceptibility with the exact solution of the quantum transfer matrix method in the half-filled case.

topics: divided differences, many-body perturbation theory (MBPT), Feynman vacuum diagrams, finite temperature

1. Introduction

One of the major scientific challenges is developing an accurate method to calculate the properties of systems with a large number of interacting particles at finite temperatures. Finding solutions to this problem is crucial not only for addressing practical issues in materials science and chemistry, but also for understanding the fundamental behaviors of interacting quantum systems. These systems, which can range from electrons in a solid to atoms in a gas, exhibit complex behaviors due to their interactions, making them difficult to model and predict. Improved computational techniques and theoretical models are needed to accurately capture these behaviors.

There are several computational methods used to study correlated systems, including exact diagonalization (ED) [1–3], dynamical mean field theory (DMFT) [4–6], density-matrix renormalization group (DMRG) [7–9], variational Monte Carlo (VMC) [10, 11], auxiliary field quantum Monte Carlo (AFQMC) [12–15], density matrix embedding theory (DMET) [16–18], and diagrammatic Monte Carlo (DiagMC) [19–21]. Each of these methods has its own strengths and limitations, making the choice of method dependent on the specific characteristics of the strongly correlated system under investigation, such as dimensionality, the nature of the correlations (local vs non-local), the desired accuracy, and the available computational resources. The major problem of the Monte-Carlo methods lies in the fermionic sign problem, which arises due to the antisymmetric nature of fermionic wavefunctions, especially in systems with strong correlations or at low temperatures. Moreover, these methods can be computationally demanding, particularly for large systems or when high precision is required. The computational cost scales with the number of particles, system size, and temperature, making it challenging to apply to complex systems or explore a wide range of parameter space.

The aim of this paper is to propose a method that does not rely on stochastic processes. This method is related to our recently developed approach that reformulates the contributions of Feynman diagrams as a divided difference [22]. To demonstrate the validity of this method, we apply it to the one-dimensional (1D) Hubbard model [23, 24]. The Hubbard model serves as a foundational framework for understanding the behavior of interacting electrons in condensed matter physics. Despite its relatively simple formulation, the model captures essential phenomena such as electron correlation, metal–insulator transitions, magnetism, and

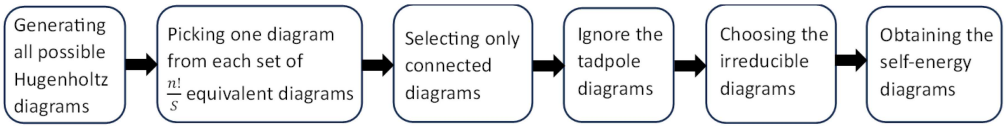

Fig. 1. Steps for reducing the number of diagrams.

unconventional superconductivity. The interplay between electron hopping and on-site interactions in the Hubbard model creates a rich landscape of phases and critical behaviors, making it a central focus for both analytical and numerical approaches in theoretical physics.

2. Overview

The general expression of the grand-canonical Hamiltonian of spin-1/2 interacting fermions under the impact of an external magnetic field h reads

$$H = \sum_{p} \left(\varepsilon_p + h\sigma - \mu\right) \hat{a}_p^\dagger \hat{a}_p + \frac{1}{4} \sum_{p_1,p_2,p_3,p_4} V_{p_3,p_4}^{p_1,p_2} \hat{a}_{p_1}^\dagger \hat{a}_{p_2}^\dagger \hat{a}_{p_4} \hat{a}_{p_3}, \tag{1}$$

where ε_p is the quasi-particle energy and μ is the chemical potential. The summation indices p_i, where $1 \leq i \leq 4$, denote the sum over momenta k_i and spins $\sigma_i = \{\uparrow, \downarrow\}$, i.e., $p_i := (k_i, \sigma_i)$. Here, $\hat{a}_p^\dagger$ and $\hat{a}_p$ are the creation and annihilation fermionic operators, respectively, which obey the anti-commutation relations $\{\hat{a}_i^+, \hat{a}_j\} = \delta_{i,j}$.

Here, the interacting potential $V_{p_3,p_4}^{p_1,p_2}$ is represented as the sum of the direct and exchange potentials.

For our case, the energy ε_p and the potential $V_{p_3,p_4}^{p_1,p_2}$ of the Hubbard model in d-dimensions [23] are defined as follows

$$\varepsilon_{k\sigma} = -2t \sum_{i=1}^{d} \cos(k_i), \tag{2}$$

$$V_{p_3,p_4}^{p_1,p_2} = U\left(\delta_{\sigma_1\sigma_3}\delta_{\sigma_2\sigma_4} - \delta_{\sigma_1\sigma_4}\delta_{\sigma_2\sigma_3}\right) \delta_{k_1+k_2,k_3+k_4}. \tag{3}$$

In order to obtain the thermodynamic properties of this system at finite temperature, we need to evaluate the grand potential Ω. This, in turn, can be expressed as a sum of the contributions from vacuum diagrams [22, 25]

$$\Omega = \Omega_{\mathrm{HF}} + \sum\nolimits_{n=2}^{\infty} \Omega_n, \tag{4}$$

where the Hartree–Fock contribution Ω_{HF} is the sum of the zeroth- and first-order terms of the grand potential series

$$\Omega_{\mathrm{HF}} = \Omega_0 + \Omega_1 = -\frac{1}{\beta} \int \mathrm{d}p \ \log\left(1 + \exp(-\beta E_p)\right) - \frac{1}{2} \iint \mathrm{d}p\, \mathrm{d}q \ V_{p,q}^{p,q} \ f^-(E_p) f^-(E_q), \tag{5}$$

where $\beta = \frac{1}{k_{\mathrm{B}} T}$, with k_{B} being the Boltzmann constant, T the temperature, and $f^{\mp}$ representing the Fermi–Dirac statistical factors

$$f^{\mp}(E_p) = \frac{\mp 1}{\mathrm{e}^{\pm\beta E_p} + 1} = \mp\frac{1}{2} + \frac{1}{2} \tanh\left(\frac{\beta}{2} E_p\right). \tag{6}$$

The integration $\int \mathrm{d}p$ in (5) indicates the sum over spins σ and momenta k, i.e., $\int \mathrm{d}p = \sum_\sigma \int \mathrm{d}k$.

The Hartree–Fock energy E_p is the sum of all the contributions of tadpole diagrams and is simplified by the self-consistent relation

$$E_{k\sigma} = \varepsilon_k + h\sigma - \mu + \sum_{\sigma'=\uparrow,\downarrow} \frac{1}{(2\pi)^d} \int_{-\pi}^{\pi} \frac{\mathrm{d}q \ \ V_{k\sigma,q\sigma'}^{k\sigma,q\sigma'}}{1 + \exp(\beta E_{q\sigma'})}, \tag{7}$$

or

$$E_{k\uparrow} = \varepsilon_k + h - \mu + U\langle n_\downarrow \rangle, \tag{8}$$

$$E_{k\downarrow} = \varepsilon_k - h - \mu + U\langle n_\uparrow \rangle. \tag{9}$$

Note that, in this work, the n-th order contribution Ω_n, where $n \geq 2$, is the sum of contributions of all N reducible vacuum diagrams that are generated at order n, i.e.,

$$\Omega_n = \sum_{i=1}^{N} \Omega_n^i. \tag{10}$$

Evaluating vacuum diagrams is not an easy task because the number of these diagrams grows factorially with increasing order n. However, several algorithms have been developed to address this problem. Among them, essentially distinct Hugenholtz diagrams (EDHD) [26] stands out as one of the fastest, as its algorithm can generate irreducible diagrams with their symmetry factors S, even at order 10, in less than 2 min using a home computer.

Figure 1 illustrates the steps used to reduce the number of diagrams that need to be evaluated. It is important to note that these diagrams are generated in the Hugenholtz representation, which can be expanded into 2^n Feynman diagrams at order n.

The approach developed in [25] offers a systematic method to compute the contribution Ω_n^i, utilizing basic algorithms in graph theory to handle the complexity of finite temperature many-body perturbation theory (MBPT).

This technique is used to analyze diagrams $G_n^i(n, 2n)$ consisting of n vertices and $2n$ edges. These edges contain a set of energies $\{E_1, E_2, \ldots, E_{2n}\}$ with associated positive integers $\{\eta_1, \eta_2, \ldots, \eta_{2n}\}$, known as edge coefficients. Within such diagrams, a set of spanning trees

can be generated. Each spanning tree, denoted as $T(n, n-1)$, encompasses all n vertices and $n-1$ edges, known as branches, of G_n^i. The primary condition for these branches is that they must not form any cycles. Following the generation of a spanning tree, the remaining $n+1$ edges of the diagram G_n^i, called chords, constitute a complementary tree denoted as $T^*(n, n+1)$. By employing this method, we get

$$\Omega_n^i = \frac{V_n^i}{S_n^i} \sum_T \frac{\prod_{j=1}^{n+1} f^{\left[\eta_j + \sum_{r_1} \eta_{r_1} - \sum_{r_2} \eta_{r_2}\right]}(E_{b_j})}{\prod_{j=1}^{n-1} \left(E_{s_j} + \sum_{r_1} E_{r_1} - \sum_{r_2} E_{r_2}\right)}, \tag{11}$$

where

$$V_n^i = \prod_{j=1}^{n} V_{p_{2j-1}, p_{2j}}^{p_{2l_j-1}, p_{2r_j}}. \tag{12}$$

The summation $\sum_T$ is carried out over all spanning trees T of the diagram $G_n^i(n, 2n)$. In each spanning tree T, the energies E_s with $1 \leq j \leq n-1$ correspond to the branches of T. Conversely, the energies E_{b_j} with $1 \leq j \leq n+1$ represent the chords of the complementary tree T^*.

The expression $\sum_{r_1} E_{r_1} \left(\sum_{r_2} E_{r_2}\right)$ symbolizes the total energy traversing the fundamental cut of the branch E_{s_j} in the same direction (or opposite direction) as E_{s_j}.

Finally, η_j, $\sum_{r_1} \eta_{r_1}$, and $\sum_{r_2} \eta_{r_2}$ denote the edge coefficients of the fundamental cycle. Here, $\sum_{r_1} \eta_{r_1}$ represents the total coefficient of the branches encountered in the same direction as η_j, while $\sum_{r_2} \eta_{r_2}$ represents the total coefficient of the branches pointed in the opposite direction to η_j. The value of $O_j = \eta_j + \sum_{r_1} \eta_{r_1} - \sum_{r_2} \eta_{r_2}$ is called the total orientation of the cycle, and the brackets $[O_j]$ within the exponent of f^{O_j} indicate its sign.

Now, the problem of integration over space and time has been reduced to integration over space only. However, another issue arises. Namely, calculating the integrals of the contribution (11) for each spanning tree individually can result in poles appearing in the denominators of (11), which could further complicate the problem. To address this, we have recently proposed an alternative algorithm [22] to overcome this difficulty. The core idea of this method is to express the contribution (11) in terms of divided differences. This technique helps to smooth these contributions and can be formulated in the following general form

$$\Omega_n^i = \frac{1}{S_n^i} \sum_{j=1}^{N_D} D_j. \tag{13}$$

Here, N_D represents the number of divided differences, where each D_j takes the following form

$$D_j = \int \mathrm{d}p \prod_{i=1}^{r} f^-[E_{p_{m_i}}, d_{i,1}^j, \ldots, d_{i,m_i}^j] \prod_{i=r+1}^{n+1} f^{\pm}[E_{p_i}], \tag{14}$$

where $f^-[x_1, x_2, ..., x_k]$ is the divided difference (see Appendix A) of the Fermi–Dirac distribution.

The energies $E_{p_{m_i}}$ represent the branches of the selected spanning tree, while $d_{i,r}^j$, where $1 \leq r \leq m_i$ can be formulated as follows

$$d_{i,r}^j - E_{p_{m_i}} = \sum_{l \in S_{\text{in}}} E_{p_l} - \sum_{l \in S_{\text{out}}} E_{p_l}. \tag{15}$$

The choice of energy indexes in the right-hand side of (15) is guided by the conservation of momentum

$$\sum_{l \in S_{\text{in}}} k_l = \sum_{l \in S_{\text{out}}} k_l. \tag{16}$$

The sets S_{in} and S_{out} represent the entered and sorted chords. The choice of m_i is fulfilled by the following relation

$$\sum_{i=1}^{r} m_i = n-1; \quad 1 \leq m_1 \leq m_2 \ldots \leq m_r \leq n-1. \tag{17}$$

The integral in (14) is overall momentum and is also a summation of the spins

$$\int \mathrm{d}p := \sum_{s_1, \ldots, s_{n+1} = \uparrow\downarrow} \int_{-\pi}^{\pi} \frac{\mathrm{d}\boldsymbol{k}_1 \, \mathrm{d}\boldsymbol{k}_2 \ldots \mathrm{d}\boldsymbol{k}_{n+1}}{(2\pi)^{(n+1)d}}. \tag{18}$$

3. Divided difference expansion at high temperature

The contribution in (14) is well-suited for constructing a high-temperature series expansion, as we can directly expand the divided difference using the expansion of the power function (see (44) in Appendix A). In this work, we present an efficient method to construct the divided difference in a factorial manner.

Using the recursive relation of the divided difference, we derive

$$f\left[d_0, d_1, d_2, ..., d_r\right] = \sum_{n=r}^{\mathrm{M}} A_n^r d_0^{n-r}, \tag{19}$$

where

$$A_n^{(0)} = -\frac{\beta^n}{n!} \frac{\partial^n}{\partial x^n} \left(\frac{1}{1+\exp(x)}\right)_{x=0}. \tag{20}$$

And for $1 \leq j \leq r$,

$$A_n^{(j)} = \sum_{i=n}^{M} A_i^{(j-1)} d_j^{i-n}. \tag{21}$$

The factored form of (21) can also be expanded using Horner's method [27], enabling an efficient construction of the divided difference via Algorithm 1.

This algorithm allows for the evaluation of the expansion of the divided difference in $O(n^3)$ operations. It improves computational efficiency while maintaining accuracy, which is particularly useful in high-temperature series expansions of complex models. This approach enables faster calculations in models such as the d-Hubbard model and can be extended to other perturbative frameworks.

Algorithm 1 Divided difference expansion at high temperature

Require: r, M
Ensure: A_r
Initialization:
for $n = r$ to M **do**
  $A_n \leftarrow a_n$
end for
Construction Loop:
for $i = 0$ to r **do**
  for $n = r$ to M **do**
    $h \leftarrow A_{\mathrm{OR}}$
    for $j = M - n - 1$ to 0 step -1 **do**
      $h \leftarrow h \cdot d_i + A_{j+n}$
    end for
    $A_n \leftarrow h$
    if $i = r$ **then**
      break
    end if
  end for
end for
return A_r

Algorithm 2 Calculate ladder diagram contribution

$u(k,q) = 1 + \tanh\left(\frac{\beta}{2}E_{q+k\uparrow}\right)\tanh\left(\frac{\beta}{2}E_{q-k\downarrow}\right)$
$v(k,q) = \frac{1}{4t\cos(q)}\left[\tanh\left(\frac{\beta}{2}E_{q+k\uparrow}\right) + \tanh\left(\frac{\beta}{2}E_{q-k\downarrow}\right)\right]$
for $n \geq 2$ **do**
  $u(k,q) \leftarrow \frac{1}{2\pi}\int_{-\pi}^{\pi} \mathrm{d}r\ \frac{u(k,q)v(r,q)-u(r,q)v(k,q)}{\cos(r)-\cos(k)}$
  $\Sigma_n^L(q) = \left(\frac{U}{2}\right)^n \frac{1}{2\pi}\int_{-\pi}^{\pi} \mathrm{d}k\ u(k,q)$
end for
Comment: The contribution of all ladder diagrams is given by:
$\Omega^L = \sum_{n=2}^{\infty} \frac{1}{2n}\frac{1}{2\pi}\int_{-\pi}^{\pi} \mathrm{d}q\ \sum_n^L(q)$

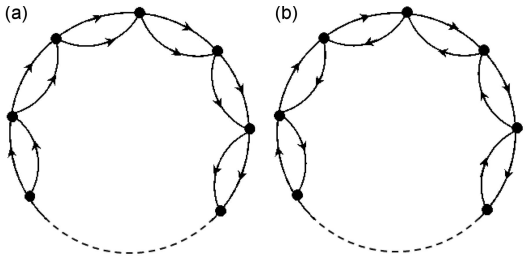

Fig. 2. The vacuum ladder-type (a) and bubble-type (b) Hugenholtz diagrams.

4. The contribution of ladder and bubble diagrams

The second-order contribution Ω_2 contains one ladder diagram, and the third-order Ω_3 contains one ladder and one bubble diagram. In this section, we see how to convert the contributions of the ladder (Fig. 2a) and bubble (Fig. 2b) diagrams.

The ladder and bubble Hugenholtz-type diagrams are more general than the ladder and bubble Feynman diagrams (the n-th order of Hugenholtz diagrams = 2^n Feynman diagrams), and these generalizations introduce more corrections in the contribution of grand potential. The general contribution of ladder Ω_n^L and bubble Ω_n^B vacuum diagrams is described in the following form (see the detailed calculation in Appendix B)

$$\Omega_n^L = \frac{\coth\left[E_{q+k_1\uparrow}+E_{q-k_1\downarrow},\ldots,E_{q+k_n\uparrow}+E_{q-k_n\downarrow}\right]}{2} \times \prod_{i=1}^{n}\frac{U}{2}\left[\tanh\left(\frac{\beta}{2}E_{q+k_i\uparrow}\right)+\tanh\left(\frac{\beta}{2}E_{q-k_i\downarrow}\right)\right], \tag{22}$$

$$\Omega_n^B = \begin{cases} \Omega_n^{B_1}, & \text{if } n \text{ odd}, \\ \Omega_n^{B_1} + \Omega_n^{B_2}, & \text{if } n \text{ even}, \end{cases} \tag{23}$$

where $\coth[x_1,\ldots,x_n]$ represents the divided difference of the function $\coth\left(\frac{\beta}{2}x\right)$, and $\Omega_n^{B_1}$ and $\Omega_n^{B_2}$ are defined as

$$\Omega_n^{B_1} = \frac{(-1)^n \coth\left(E_{k_1+q\uparrow}-E_{k_1-q\downarrow},\ldots,E_{k_n+q\uparrow}-E_{k_n-q\downarrow}\right)}{2}\prod_{i=1}^{n}\frac{U}{2}\left[\tanh\left(\frac{\beta}{2}E_{k_i+q\uparrow}\right)-\tanh\left(\frac{\beta}{2}E_{k_i-q\downarrow}\right)\right], \tag{24}$$

$$\Omega_n^{B_2} = \frac{\coth\left(E_{k_1+q\uparrow}-E_{k_1-q\uparrow},\ldots,E_{k_n+q\downarrow}-E_{k_n-q\downarrow}\right)}{2}\prod_{i=1}^{\frac{n}{2}}\left(\frac{U}{2}\right)^2\left[\tanh\left(\frac{\beta}{2}E_{k_{2i-1}+q\uparrow}\right)-\tanh\left(\frac{\beta}{2}E_{k_{2i-1}-q\uparrow}\right)\right] \times\left[\tanh\left(\frac{\beta}{2}E_{k_{2i}+q\downarrow}\right)-\tanh\left(\frac{\beta}{2}E_{k_{2i}-q\downarrow}\right)\right]. \tag{25}$$

In order to calculate the integrals of the ladder contribution, (22), and the bubble contribution, (23), over the momentum in a recursive manner, we utilize the multidimensional divided difference integration algorithm (see Algorithm 4 in Appendix A).

Algorithm 3 Calculate bubble diagram contribution

$u_1(k,q)=1-\tanh\left(\frac{\beta}{2}E_{k+q\uparrow}\right)\tanh\left(\frac{\beta}{2}E_{k-q\downarrow}\right)$
$v_1(k,q)=\frac{1}{4t\sin(q)}\left[\tanh\left(\frac{\beta}{2}E_{k+q\uparrow}\right)-\tanh\left(\frac{\beta}{2}E_{k-q\downarrow}\right)\right]$
$u_2(k,q,s)=1-\tanh\left(\frac{\beta}{2}E_{k+qs}\right)\tanh\left(\frac{\beta}{2}E_{k-qs}\right)$
$v_2(k,q,s)=\frac{1}{4t\sin(q)}\left[\tanh\left(\frac{\beta}{2}E_{k+qs}\right)-\tanh\left(\frac{\beta}{2}E_{k-qs}\right)\right]$
for $n\geq 2$ **do**
  $u_1(q,k)\leftarrow\frac{1}{2\pi}\int_{-\pi}^{\pi}\mathrm{d}r\ \frac{u_1(k,q)v_1(r,q)-u_1(r,q)v_1(k,q)}{\sin(r)-\sin(k)}$
  $\sum_n^{(B_1)}(q)=(-U/2)^n\frac{1}{2\pi}\int_{-\pi}^{\pi}\mathrm{d}k\ u_1(k,q)$
  if n even **then**
    $u_2(k,q,\uparrow)\leftarrow\frac{1}{2\pi}\int_{-\pi}^{\pi}\mathrm{d}r\ \frac{1}{\sin(k)-\sin(r)}\times\left[u_2(k,q,\uparrow)v_2(r,q,\downarrow)-u_2(r,q,\downarrow)v_2(k,q,\uparrow)\right]$
    $u_2(k,q,\downarrow)\leftarrow\frac{1}{2\pi}\int_{-\pi}^{\pi}\mathrm{d}r\ \frac{1}{\sin(k)-\sin(r)}\times\left[u_2(k,q,\downarrow)v_2(r,q,\uparrow)-u_2(r,q,\uparrow)v_2(k,q,\downarrow)\right]$
    $\sum_n^{(B_2)}(q)=\frac{1}{2}\left(\frac{U}{2}\right)^n\frac{1}{2\pi}\int_{-\pi}^{\pi}\mathrm{d}k\times[u_2(k,q,\uparrow)+u_2(k,q,\downarrow)]$
  else
    $u_2(k,q,s)\leftarrow\frac{1}{2\pi}\int_{-\pi}^{\pi}\mathrm{d}r\ \frac{1}{\sin(k)-\sin(r)}\times\left[u_2(k,q,s)v_2(r,q,s)-u_2(r,q,s)v_2(k,q,s)\right]$
    $\sum_n^{(B_2)}(q)=0$
  end if
end for
Comment: The bubble diagram contribution is:
$\Omega^B=\sum_{n=3}^{\infty}\frac{1}{2n}\frac{1}{2\pi}\int_{-\pi}^{\pi}\mathrm{d}q\ \left(\sum_n^{(B_1)}(q)+\sum_n^{(B_2)}(q)\right)$

Algorithm 2 summarizes the general steps for integrating over the momentum in the ladder contribution given by (22).

The recursive integration method of the bubble contribution Ω^B is defined by Algorithm 3.

Algorithms 2 and 3 can be utilized to evaluate the contributions of ladder and bubble diagrams for any temperature, including $T=0$. They can also be used to efficiently evaluate these contributions at high temperatures.

5. High-temperature series expansions

The coupled non-linear integral Hartree–Fock equations (8) and (9) can be solved numerically for a given temperature. At high temperature, we can find the series expansion of $E_{p\downarrow}(\beta)$ and $E_{p\uparrow}(\beta)$ around β. In this case, we define these energies in the form of the following polynomials

$$E_{p\downarrow}(\beta)=-2t\cos(p)+\sum_{i=0}^{\infty}a_i\beta^i,$$
$$E_{p\uparrow}(\beta)=-2t\cos(p)+\sum_{i=0}^{\infty}b_i\beta^i. \tag{26}$$

To obtain the coefficients a_i and b_i in a recursive manner, we replace the polynomials $E_{p\downarrow}(\beta)$ and $E_{p\uparrow}(\beta)$ in (26) and apply the Maclaurin series expansion of the function tanh around β.

The initial values used are

$$a_0=v_1=-h-\mu+\frac{U}{2},$$
$$b_0=v_2=h-\mu+\frac{U}{2}, \tag{27}$$

and for $i\geq 1$

$$a_i=-\frac{U}{4\pi}\int_{-\pi}^{\pi}\frac{\mathrm{d}k}{i!}\left[\frac{\partial^i}{\partial\beta^i}\tanh\left(\frac{\beta}{2}\sum_{j=0}^{i-1}b_j\beta^j\right)\right]_{\beta=0},$$
$$b_i=-\frac{U}{4\pi}\int_{-\pi}^{\pi}\frac{\mathrm{d}k}{i!}\left[\frac{\partial^i}{\partial\beta^i}\tanh\left(\frac{\beta}{2}\sum_{j=0}^{i-1}a_j\beta^j\right)\right]_{\beta=0}. \tag{28}$$

By applying the recursive form (28), we can derive the high-temperature series expansions of the Hartree–Fock energies $E_{p\downarrow}(\beta)$ and $E_{p\uparrow}(\beta)$ up to any desired order. We provide the first four orders,

$$E_{p\sigma}=-2t\cos(p)+A_\sigma, \tag{29}$$

where

$$A_\downarrow=v_1-\frac{\beta}{4}Uv_2+\frac{\beta^2}{16}U^2v_1+\frac{\beta^3}{192}Uv_2(24t^2-3U^2+4v_2^2)+\ldots,$$
$$A_\uparrow=v_2-\frac{\beta}{4}Uv_1+\frac{\beta^2}{16}U^2v_2+\frac{\beta^3}{192}Uv_1(24t^2-3U^2+4v_1^2)+\ldots. \tag{30}$$

The zeroth-order contributions (5) at high temperature can now be written in the following form

$$\Omega_0=-\sum_{\sigma=\uparrow,\downarrow}\Omega_0^\sigma, \tag{31}$$

where

$$\Omega_0^\sigma=\frac{\ln(2)}{\beta}-\frac{A_\sigma}{2}+\frac{\beta}{8}(2+A_\sigma^2)-\frac{\beta^3}{32}\left(1+2A_\sigma^2+\frac{A_\sigma^4}{6}\right)+\beta^5\left(\frac{1}{144}+\frac{A_\sigma^2}{32}+\frac{A_\sigma^4}{96}+\frac{A_\sigma^6}{2880}\right)+\ldots. \tag{32}$$

Moreover, for the first order, we have

$$\langle n_\sigma\rangle=\frac{1}{2}-\frac{\beta A_\sigma}{4}+\frac{\beta^3}{48}(6A_\sigma+A_\sigma^3)-\frac{\beta^5}{480}(30A_\sigma+20A_\sigma^3+A_\sigma^5)+\ldots. \tag{33}$$

The high-temperature series of the first-order contribution Ω_1 is obtained simply by substituting $\langle n_\sigma\rangle$ into (5). The Hartree–Fock part's contribution Ω^{HF} can be determined by substituting the series of A_σ from (33) into both the zeroth-order Ω_0 and the first-order Ω_1, i.e.,

$$\Omega^{\mathrm{HF}}=\Omega_0+\Omega_1=-\frac{2\ln(2)}{\beta}+\frac{1}{4}(-U+2v_1+2v_2)-\frac{\beta}{8}(4t^2+v_1^2+v_2^2)+\frac{\beta^2}{16}Uv_1v_2+\ldots. \tag{34}$$

The ladder Ω^L and bubble Ω^B contributions at high temperature can be easily evaluated using the recursive algorithms, i.e., Algorithm 2 and Algorithm 3.

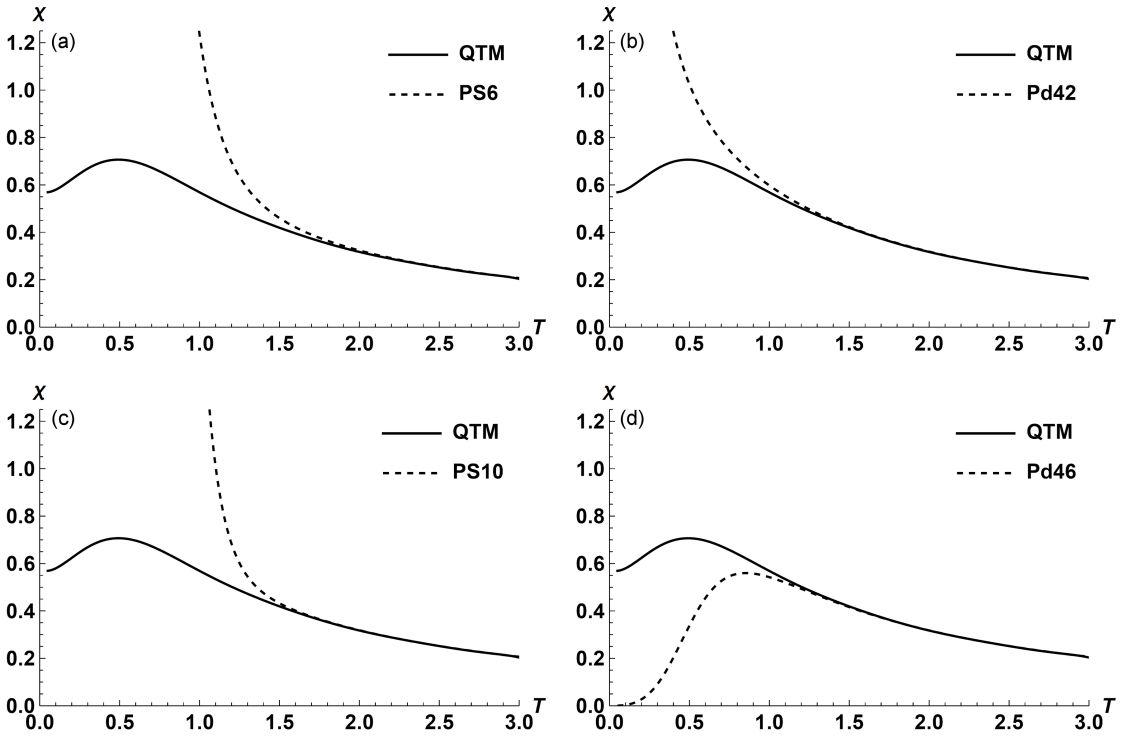

Fig. 3. Comparison of our magnetic susceptibility series (dashed line) with those obtained from the exact QTM method [29] (solid line) in the half-filled case for $t = 1$ and $U = 4$. (a) Padé approximation (4,2) of the plain series of χ derived from (37). (b) Plain series (PS10) of χ derived from (66) in Appendix C. (c) Padé approximation (4, 6) of the plain series of χ derived from (66) in Appendix C.

The first terms are

$$\Omega^L = -\frac{\beta U^2}{32} + \frac{\beta^2 U^3}{192} + \frac{\beta^3 U^2}{3072}\big(64t^2 - 3U^2 + 24A_1^2 + 24A_2^2\big) + \beta^4\left[\frac{U^5}{5120} - \frac{U^3}{768}\Big(4t^2 + A_1^2 - A_1A_2 + A_2^2\Big)\right] + \ldots, \tag{35}$$

$$\Omega^B = -\frac{\beta^2 U^3}{192} - \frac{\beta^3 U^4}{512} + \beta^4\left[-\frac{U^5}{5120} + \frac{U^3}{768}(4t^2 + A_1^2 + A_1A_2 + A_2^2)\right] + \frac{\beta^5 U^4}{12288}\Big(32t^2 - U^2 + 10A_1^2 + 4A_1A_2 + 10A_2^2\Big) + \ldots. \tag{36}$$

Note that the contributions of the second Ω_2 and the third Ω_3 are included in Ω^L and Ω^B. By implementing the recursive algorithms (Algorithm 2 and Algorithm 3) in Mathematica, we can reach the order of 50 in both U and β in less than 2 min using a home computer.

6. Results

By substituting the Hartree–Fock, and ladder and bubble contributions, and applying the general integration process to other diagrams, we obtain the grand potential up to the sixth order in terms of the many-body potential U^6 and up to the sixth order in terms of the inverse temperature β^6, i.e.,

$$\Omega = -\frac{2\ln(2)}{\beta} + \left(\frac{c_1}{2} - \frac{U}{4}\right) - \frac{\beta}{8}\left(c_1^2 + 4t^2 + \frac{U^2}{4}\right) + \frac{\beta^2}{16}c_2U + \frac{\beta^3}{192}\left(c_1^4 + 12c_1^2t^2 + 12t^4 + 4t^2U^2 + \frac{U^4}{16}\right) - \frac{\beta^4 c_2 U}{192}\left(c_1^2 + 12t^2 + \frac{U^2}{4}\right) + \frac{\beta^5}{5760}\left[\frac{45c_2^2U^2}{4} - 2c_1^6 - 60c_1^4t^2 - 80t^6 - \frac{153t^4U^2}{2} - \frac{9t^2U^4}{2} - \frac{U^6}{32} - 30c_1^2t^2\Big(6t^2 + \frac{U^2}{4}\Big)\right] + \frac{\beta^6 c_2 U}{11520}\left[6c_1^4 + 5c_2^2 + 5c_1^2\left(30t^2 + \frac{U^2}{4}\right) + 6\left(90t^4 + \frac{15t^2U^2}{2} + \frac{U^4}{16}\right)\right], \tag{37}$$

where

$$c_1^p = v_1^p + v_2^p = \left(h-\mu+\frac{U}{2}\right)^p + \left(-h-\mu+\frac{U}{2}\right)^p,$$
$$c_2^p = v_1^p v_2^p = \left[\left(\frac{U}{2}-\mu\right)^2 - h^2\right]^p. \tag{38}$$

From the grand potential series (37), we can derive any physical quantity for the 1D Hubbard model at high temperatures. Additionally, it is clear that the coefficients in the expansion of Ω with respect to β remain valid for any set of constants (t, U, μ, h) within this model.

Our series completely agrees with article [28] up to the fourth order β^4. The fifth and sixth orders in our results are novel and can enhance the series expansion of the grand potential at high temperatures of the 1D Hubbard model.

We can extend the results up to the tenth order in terms of β and up to the sixth order in U (see Appendix C).

The comparison of the magnetic susceptibility $\chi = -\frac{\partial^2 \Omega}{\partial h^2}|_{h=0}$ for the half-filled case $\mu = \frac{U}{2}$ with the exact results of Jüttner [29], obtained using the quantum transfer matrix method, yields better results.

In Fig. 3a, we present our plain series (PS6) of χ up to the sixth order, along with those obtained with the exact quantum transfer matrix (QTM) method. The PS6 series is further enhanced by the Padé approximation in Fig. 3b. From both figure panels, we can conclude that our results demonstrate a better approximation of the magnetic susceptibility.

In Fig. 3c and d, we illustrate a significant improvement in the magnetic susceptibility of the plain series (PS10) and its Padé approximation derived from the grand potential (65) in Appendix C. From these figure panels, we can conclude that further expansion in β will enhance the expansion of the grand potential.

The high-temperature expansion of the grand potential for the one-dimensional Hubbard model has been implemented in the Mathematica language. The main code is available on our GitHub page, see [30].

7. Conclusions

In this paper, a novel solution of the one-dimensional Hubbard model is presented, using our recently developed many-body perturbation theory [22]. This method allows us to derive the analytic expressions of the coefficients of the high-temperature series expansion (HTSE) of the grand potential at each order. Unlike other traditional methods, the proposed method can easily evaluate the coefficients of HTSE up to order 10 or higher in terms of β, as mentioned above.

In this context, we proposed a new algorithm to evaluate the expansion of the divided difference at high temperature in $\mathcal{O}(n^3)$ operations with the help of Horner's method.

Additionally, this method assists in deriving a recursive calculation of the contributions from ladder and bubble vacuum diagrams.

For this purpose, we developed symbolic code in the Mathematica language to assist us in implementing this method. This code can be used to evaluate the series expansion up to the desired order without worrying about the evaluation time.

To determine the range of validity in β of our analytical solution for the grand potential per site for different values of U in units of t, we considered the curves of the magnetic susceptibility for $U = 4$ at half-filling case. The plotted curve of the susceptibility coincides completely with the exact solution of Jüttner et al. [29] for $T \geq 1.1$ with the help of the Padé approximation.

Finally, we should mention that the present approach is applicable for low temperatures and is also ready for the two- and three-dimensional Hubbard model. We will report such possibilities together in the near future.

Appendix A: Divided differences

Divided differences are an essential tool in numerical analysis and interpolation, utilized to create polynomial approximations of functions. They play a crucial role in techniques like Newton's divided difference interpolation formula.

The first-order divided difference $f[x_0, x_1]$ between two points, $(x_0, f(x_0))$ and $(x_1, f(x_1))$, is defined by the following fraction

$$f[x_0, x_1] = \frac{f(x_0) - f(x_1)}{x_0 - x_1}. \tag{39}$$

In general, the k-th divided difference involving $k+1$ points $(x_0, f(x_0))$, $(x_1, f(x_1))$, ..., $(x_k, f(x_k))$ is defined as follows

$$f[x_0, x_1, \ldots, x_k] = \frac{f[x_1, \ldots, x_k] - f[x_0, \ldots, x_{k-1}]}{x_k - x_0}, \tag{40}$$

where $f[x_i, x_{i+1}, \ldots, x_j]$ represents the $(j-i)$-th divided difference for the points $x_i, x_{i+1}, \ldots, x_j$.

The base case for the divided differences are the function values themselves $f[x_i] = f(x_i)$.

An alternative definition of the divided difference is

$$f[x_0, x_1, \ldots, x_k] = \sum_{i=0}^{k} \frac{f(x_i)}{\prod_{j \neq i}(x_i - x_j)}. \tag{41}$$

In this work, we use the term "modified divided difference" for the following formula

$$f[g; x_0, x_1, \ldots, x_k] = \sum_{i=0}^{k} f(x_i) \prod_{j \neq i} \frac{g(x_j)}{(x_i - x_j)}. \tag{42}$$

The recursive formula for the modified divided difference is defined as follows

$$f\left[g;x_0,\ldots,x_k\right]=\frac{f\left[g;x_0,\ldots,x_{k-1}\right]g\left(x_k\right)-f\left[g;x_1,\ldots,x_k\right]g\left(x_0\right)}{x_0-x_k}, \tag{43}$$

where $f[g;x]=f[x]$.

By definition, divided differences remain unchanged under any permutation of the variables $x_0,x_1,\ldots,x_k$. This means that the value of the divided difference does not depend on the order in which the variables $x_0,x_1,\ldots,x_k$ are arranged.

The Taylor series expansion of the divided differences can be derived using the definition of divided differences and properties of the Taylor series.

For a function f that is sufficiently smooth; the k-th divided difference for points $x_0,x_1,\ldots,x_k$ can be expressed using the derivatives of f. The formula is

$$f[x_0,x_1,\ldots,x_k]=\sum_{n=k}^{\infty}\frac{f^{(n)}(0)}{n!}x_0^{i_0}x_1^{i_1}\ldots x_k^{i_k}, \tag{44}$$

where the integers $i_j\geq 0$, where $0\leq j\leq k$, are selected according to the following condition

$$\sum\nolimits_{j=0}^{k} i_j=n-k. \tag{45}$$

The integral representation of the Hermite–Genocchi formula for divided differences is given by

$$f[x_0,x_1,\ldots,x_k]=\int_0^1 \mathrm{d}t_1\int_0^{t_1}\mathrm{d}t_2\ldots\int_0^{t_{k-1}}\mathrm{d}t_k\;\; f^{(k)}\big((1-t_1)x_0+\ldots+(t_{k-1}-t_k)x_{k-1}+t_kx_k\big). \tag{46}$$

Algorithm 4 Calculate Integral I

1: Set $u=f(x(p))$
2: **for** $1\leq i\leq k$ **do**
3: $\quad u(x(p))=\int \mathrm{d}q\;\frac{u(x(p))-u(x(q))}{x(p)-x(q)}$
4: **end for**
5: The output result is $I=\int \mathrm{d}p\;u(x(p))$

Algorithm 5 Calculate integral I

1: Set $u=f(x(p))$
2: **for** $1\leq i\leq k$ **do**
3: $\quad u(x(p))=\int \mathrm{d}q\;\frac{u(x(p))g(x(q))-u(x(q))g(x(p))}{x(p)-x(q)}$
4: **end for**
5: The output result is $I=\int \mathrm{d}p\;u(x(p))$

Here, the integration is carried out over the simplex defined by $0\leq t_1\leq t_2\leq\cdots\leq t_k\leq 1$. This integral representation expresses the k-th divided difference in terms of the k-th derivative of the function f, integrated over a weighted average of the points $x_0,x_1,\ldots,x_k$.

To evaluate the following integrals of the divided differences

$$I=\int \mathrm{d}p_0\ldots\int \mathrm{d}p_k\;\; f\big[x(p_0),x(p_1),\ldots,x(p_k)\big], \tag{47}$$

we can utilize the following recursive algorithm, namely Algorithm 4.

For the integrals involving modified divided differences

$$I=\int \mathrm{d}p_0\ldots\int \mathrm{d}p_k\;\; f\big[g;x(p_0),x(p_1),\ldots,x(p_k)\big], \tag{48}$$

we implement the subsequent recursive algorithm, namely Algorithm 5.

Appendix B: The general contribution of Ladder and bubble vacuum diagrams

Following the process outlined in algorithm presented in [25], we can deduce that the general contribution of ladder diagrams is described in the following form

$$\Omega_n^L=V^+\sum_{i=1}^{n}f^-(x_{2j-1})f^-(x_{2i})\times\prod_{j\neq i}^{n}\left(\frac{f^-(x_{2j-1})+f^+(x_{2j})}{x_{2i-1}+x_{2i}-x_{2j-1}-x_{2j}}\right), \tag{49}$$

where the general potential V^+ is given by

$$V^+=\frac{U^n}{4^n}V_{p_1,p_2}^{p_{2n-1},p_{2n}}\prod_{i=1}^{n-1}V_{p_{2i+1},p_{2i+2}}^{p_{2i-1},p_{2i}}. \tag{50}$$

The contribution (49) can be expressed as follows

$$\Omega_n^L=V^+\sum_{i=1}^{n}\frac{f^-(x_{2j-1})f^-(x_{2i})\prod_{j=1}^{n}\Big(f^-(x_{2j-1})+f^+(x_{2j})\Big)}{\Big(f^-(x_{2i-1})+f^+(x_{2i})\Big)\prod_{j\neq i}^{n}(x_{2i-1}+x_{2i}-x_{2j-1}-x_{2j})}. \tag{51}$$

Using the Fermi distribution relations (6), we have

$$\frac{f^-(x_{2i-1})f^-(x_{2i})}{f^-(x_{2i-1})+f^+(x_{2i})} = \frac{1}{\mathrm{e}^{\beta(x_{2i-1}+x_{2i})}-1} = B(x_{2i-1}+x_{2i}). \tag{52}$$

After replacing the function B with its relation (52) in the contribution (51), we find

$$\Omega_n^L = V^+ \sum_{i=1}^{n} B(x_{2i-1}+x_{2i}) \times \prod_{j\neq i}^{n}(x_{2i-1}+x_{2i}-x_{2j-1}-x_{2j}) \times \prod_{j=1}^{n}\big(f^-(x_{2j-1})+f^+(x_{2j})\big). \tag{53}$$

Now, replacing the sum in (53) with the identity of the divided difference (42) yields

$$\Omega_n^L = V^+ B[x_1+x_2, x_3+x_4, \ldots, x_{2n-1}+x_{2n}] \times \prod_{j=1}^{n}\Big(f^-(x_{2j-1})+f^+(x_{2j})\Big). \tag{54}$$

By substituting the potential V^+ in (50) and replacing $x_i{=}E_{p_i}{=}E_{k_i\sigma_i}$, then summing over spins σ_i, we find

$$\Omega_n^L = U^n \coth[E_{k_1\uparrow}+E_{k_2\downarrow}, \ldots, E_{k_{2n-1}\uparrow}+E_{k_{2n}\downarrow}] \times \prod_{j=1}^{n}(f^-(E_{k_{2j-1}\uparrow})+f^+(E_{k_{2j}\downarrow}))\delta_{k_{2j-1}+k_{2j},k_1+k_2} \tag{55}$$

We can change the variables in (55) according to the conservation of momentum $\prod_{j=1}^{n}\delta_{k_{2j-1}+k_{2j},k_1+k_2}$ as follows

$$\frac{k_{2i-1}+k_{2i}}{2} = q \qquad \frac{k_{2i-1}-k_{2i}}{2} = k_i. \tag{56}$$

Finally, by using the new momentum variables (56) and replacing $f^{\mp}(x)$ by its relation (6), we find the contribution of the ladder in the following form

$$\Omega_n^L = \frac{\coth\left[E_{q+k_1\uparrow}+E_{q-k_1\downarrow}, \ldots, E_{q+k_n\uparrow}+E_{q-k_n\downarrow}\right]}{2} \times \prod_{i=1}^{n}\frac{U}{2}\left[\tanh\left(\frac{\beta}{2}E_{q+k_i\uparrow}\right)+\tanh\left(\frac{\beta}{2}E_{q-k_i\downarrow}\right)\right], \tag{57}$$

where $\coth[x_1, \ldots, x_n]$ represents the divided difference of the function $\coth(\frac{\beta}{2}x)$.

Using the same approach, the contribution of bubble diagrams can be expressed as follows

$$\Omega_n^B = V^- \sum_{i=1}^{n} f^+(x_{2i-1})f^-(x_{2i}) \prod_{j\neq i}^{n}\frac{f^-(x_{2j-1})-f^-(x_{2j})}{(x_{2i}-x_{2i-1})-(x_{2j}-x_{2j-1})} = V^- \sum_{i=1}^{n}\left(\frac{f^+(x_{2i-1})f^-(x_{2i})}{f^-(x_{2j-1})-f^-(x_{2j})}\right)\frac{\prod_{j=1}^{n}(f^-(x_{2j-1})-f^-(x_{2j}))}{\prod_{j\neq i}^{n}\big(x_{2i}-x_{2i-1}\big)-\big(x_{2j}-x_{2j-1}\big)}, \tag{58}$$

where

$$V^- = \frac{1}{2^{n+1}}V_{p_1,p_{2n}}^{p_{2n-1},p_2}\prod_{i=1}^{n-1}V_{p_{2i+1},p_{2i}}^{p_{2i-1},p_{2i+2}} \tag{59}$$

and

$$\frac{f^+(x_{2i-1})f^-(x_{2i})}{f^-(x_{2j-1})-f^-(x_{2j})} = \Big[\mathrm{e}^{\beta(x_{2i}-x_{2i-1})}-1\Big]^{-1} = B(x_{2i}-x_{2i-1}). \tag{60}$$

Utilizing the identity of the divided difference given by (42), we find

$$\Omega_n^B = V^- B\big[-x_1+x_2, \ldots, -x_{2n-1}+x_{2n}\big] \times \prod_{j=1}^{n}(f^-\big(x_{2j-1}\big)-f^-(x_{2j})). \tag{61}$$

By substituting the potential V^- and x_i with $x_i = E_{p_i} = E_{k_i\sigma_i}$, and considering the conservation of momentum in the potential $\delta_{k_1+k_4,k_2+k_3}$ $\delta_{k_3+k_6,k_4+k_5}\ldots\delta_{k_{2n-1}+k_2,k_1+k_{2n}}$, we can change the momentum variables as follows

$$\frac{k_{2i}+k_{2i-1}}{2} = k_i, \qquad \frac{k_{2i}-k_{2i-1}}{2} = q. \tag{62}$$

After summing over spins, we encounter two states of Ω_n^B

$$\Omega_n^B = \begin{cases} \Omega_n^{B_1}, & \text{if } n \text{ odd}, \\ \Omega_n^{B_1}+\Omega_n^{B_2}, & \text{if } n \text{ even}, \end{cases} \tag{63}$$

where $\Omega_n^{B_1}$ and $\Omega_n^{B_2}$ are defined by the following forms

$$\Omega_n^{B_1} = \frac{(-1)^n}{2}\coth\left[E_{k_1+q\uparrow}-E_{k_1-q\downarrow}, \ldots, E_{k_n+q\uparrow}-E_{k_n-q\downarrow}\right]\prod_{i=1}^{n}\frac{U}{2}\left[\tanh\left(\frac{\beta}{2}E_{k_i+q\uparrow}\right)-\tanh\left(\frac{\beta}{2}E_{k_i-q\downarrow}\right)\right], \tag{64}$$

$$\Omega_n^{B_2} = \frac{1}{2}\coth\left[E_{k_1+q\uparrow}-E_{k_1-q\uparrow}, E_{k_2+q\downarrow}-E_{k_2-q\downarrow}, \ldots, E_{k_{n-1}+q\uparrow}-E_{k_{n-1}-q\uparrow}, E_{k_n+q\downarrow}-E_{k_n-q\downarrow}\right] \times \prod_{i=1}^{\frac{n}{2}}\left(\frac{U}{2}\right)^2\left[\tanh\left(\frac{\beta}{2}E_{k_{2i-1}+q\uparrow}\right)-\tanh\left(\frac{\beta}{2}E_{k_{2i-1}-q\uparrow}\right)\right]\left[\tanh\left(\frac{\beta}{2}E_{k_{2i}+q\downarrow}\right)-\tanh\left(\frac{\beta}{2}E_{k_{2i}-q\downarrow}\right)\right]. \tag{65}$$

Appendix C: Grand potential up to order 10

The grand potential is expanded up to the sixth order in terms of the many-body perturbation potential U^6 and up to ther tenth order in terms of the inverse of temperature β^{10}

$$\begin{aligned}\Omega = &-\frac{2\log(2)}{\beta}+\frac{c_1}{2}-\frac{1}{8}\beta\left(4t^2+c_1^2\right)+\frac{1}{192}\beta^3\left(12t^4+12t^2c_1^2+c_1^4\right)-\frac{\beta^5}{2880}\left(40t^6+90t^4c_1^2+30t^2c_1^4+c_1^6\right)\\
&+\frac{17\beta^7}{645120}\left(140t^8+560t^6c_1^2+420t^4c_1^4+56t^2c_1^6+c_1^8\right)-\frac{31\beta^9}{14515200}\left(504t^{10}+3150t^8c_1^2+4200t^6c_1^4\right.\\
&\left.+1260t^4c_1^6+90t^2c_1^8+c_1^{10}\right)+\frac{U}{4}\left[-1+\frac{\beta^2c_2}{4}-\frac{\beta^4c_2}{48}\left(12t^2+c_1^2\right)+\frac{\beta^6c_2}{2880}\left(540t^4+150t^2c_1^2+6c_1^4+5c_2^2\right)\right.\\
&+\frac{\beta^8c_2}{241920}\left(-29400t^6-2394t^2c_1^4-1680t^2c_2^2-51c_1^6-42c_1^2\left(405t^4+c_2^2\right)\right)+\frac{\beta^{10}c_2}{14515200}\left(1045800t^8\right.\\
&\left.\left.+1029000t^6c_1^2+306180t^4c_1^4+207900t^4c_2^2+23850t^2c_1^6+15750t^2c_1^2c_2^2+310c_1^8+252c_2^4+255c_1^4c_2^2\right)\right]\\
&+\frac{U^2\beta}{16}\left[-\frac{1}{2}+\frac{t^2\beta^2}{3}+\frac{\beta^4}{480}\left(-102t^4-10t^2c_1^2+15c_2^2\right)+\frac{\beta^6}{20160}\left(2480t^6+756t^4c_1^2-105c_1^2c_2^2\right.\right.\\
&\left.+70t^2\left(c_1^4-30c_2^2\right)\right)+\frac{\beta^8}{1451520}\left(-96740t^8-59760t^6c_1^2-14742t^4c_1^4-714t^2c_1^6+247212t^4c_2^2\right.\\
&\left.\left.+42210t^2c_1^2c_2^2+1260c_2^4+1071c_1^4c_2^2\right)\right]+\frac{U^3\beta^4c_2}{768}\left[-1+\frac{\beta^2}{12}\left(36t^2+c_1^2\right)+\frac{\beta^4}{5040}\left(-22932t^4-2520t^2c_1^2\right.\right.\\
&\left.\left.-42c_1^4+280c_2^2\right)+\frac{\beta^6}{20160}\left(101888t^6+25536t^4c_1^2+1764t^2c_1^4+17c_1^6-7560t^2c_2^2-301c_1^2c_2^2\right)\right]\\
&+\frac{U^4\beta^3}{256}\left[\frac{1}{12}-\frac{t^2\beta^2}{5}+\frac{\beta^4}{1680}\left(442t^4+14t^2c_1^2-35c_2^2\right)+\frac{\beta^6}{90720}\left(-23864t^6-2754t^4c_1^2-126\left(c_1^4-96c_2^2\right)t^2\right.\right.\\
&\left.\left.+315c_1^2c_2^2\right)\right]+\frac{U^5\beta^6c_2}{30720}\left[1-\frac{\beta^2}{12}\left(68t^2+c_1^2\right)-\frac{\beta^4}{10080}\left(-140040t^4-8330t^2c_1^2-84c_1^4+1505c_2^2\right)\right]\\
&+\frac{U^6\beta^5}{92160}\left[-\frac{1}{2}+\frac{17t^2\beta^2}{7}+\frac{\beta^4}{1344}\left(-7130t^4-102t^2c_1^2+357c_2^2\right)\right].\end{aligned} \tag{66}$$

References

[1] H.Q. Lin, *Phys. Rev. B* **42**, 6561 (1990).

[2] A. Weiße, H. Fehske, in: *Computational Many-Particle Physics, Lecture Notes in Physics*, Vol. 739, Springer, 2008 p. 529.

[3] J.M. Zhang, R.X. Dong, *Eur. J. Phys.* **31**, 591 (2010).

[4] P. Sun, G. Kotliar, *Phys. Rev. B* **66**, 085120 (2002).

[5] K. Held, *Adv. Phys.* **56**, 829 (2007).

[6] H. Park, K. Haule, G. Kotliar, *Phys. Rev. Lett.* **101**, 186403 (2008).

[7] S.R. White, *Phys. Rev. Lett.* **69**, 2863 (1992).

[8] S.R. White, *Phys. Rev. B* **48**, 10345 (1993).

[9] Y.-F. Jiang, J. Zaanen, T.P. Devereaux, H.-C. Jiang, *Phys. Rev. Res.* **2**, 033073 (2020).

[10] H. Yokoyama, H. Shiba, *J. Phys. Soc. Jpn.* **56**, 1490 (1987).

[11] K. Ido, T. Ohgoe, M. Imada, *Phys. Rev. B* **97**, 045138 (2018).

[12] H. Shi, S. Zhang, *Phys. Rev. B* **88**, 125132 (2013).

[13] S. Zhang, in: *Emergent Phenomena in Correlated Matter Modeling and Simulation*, Vol. 3, Eds. E. Pavarini, E. Koch, U. Schollwöck, Verlag des Forschungszentrums Jülich, 2013 p. 1.

[14] M. Motta, S. Zhang, *Wiley Interdiscip. Rev. Comput. Mol. Sci.* **8**, e1364 (2018).

[15] F.D. Malone, S. Zhang, M.A. Morales, *J. Chem. Theory Comput.* **15**, 256 (2019).

[16] G. Knizia, G.K.L. Chan, *Phys. Rev. Lett.* **109**, 186404 (2012).

[17] G. Knizia, G.K.L. Chan, *J. Chem. Theory Comput.* **9**, 1428 (2013).

[18] B.-X. Zheng, G.K.-L. Chan, *Phys. Rev. B* **93**, 035126 (2016).

[19] N. V. Prokof'ev, B.V. Svistunov, *Phys. Rev. Lett.* **81**, 2514 (1998).

[20] K. Van Houcke, E. Kozik, N. Prokof'ev, B. Svistunov, *Phys. Proc.* **6**, 95 (2010).

[21] Y. Deng, E. Kozik, N.V. Prokof'ev, B.V. Svistunov, *Europhys. Lett.* **110**, 57001 (2015).

[22] M.A. Tag, A. Boudiar, M.E.H. Mansour, A. Hafdallah, C. Bendjeroudib, B. Zaidi, *Phys. Scr.* **99**, 065993 (2024).

[23] J. Hubbard, *Proc. R. Soc. A* **276**, 238 (1963).

[24] M.C. Gutzwiller, *Phys. Rev. Lett.* **10**, 159 (1963).

[25] M. Tag, M. Mansour, *Int. J. Mod. Phys. C* **30**, 1950100 (2019).

[26] M. Tag, S. Khène, *Int. J. Mod. Phys. C* **28**, 1750113 (2017).

[27] T.H. Cormen, C.E. Leiserson, R.L. Rivest, C. Stein, *Introduction to Algorithms*, 3rd ed., MIT Press, 2009, p. 41; p. 900; p. 990.

[28] I. Charret, E. Silva, S. de Souza, O. Santos, M.T. Thomaz, A.T. Costa Jr., *Phys. Rev. B* **64**, 195127 (2001).

[29] G. Jüttner, A. Klümper, J. Suzuki, *Nucl. Phys. B* **522**, 471 (1998).

[30] M.A. Tag, High Temperature Series Expansion of 1D Hubbard Model, 2025.